The Sand Trapping Trench As A Countermeasure to Control Wind-Blown Sand on Beaches

Shintaro Hotta [1] Katsumori Hatanaka[1],
Hiroyoshi Tanaka [2] and Kiyoshi Horikawa [3]

Abstract

The sand trapping trench for controlling wind-blown sand is proposed and general functioning, evaluation of sand trapping efficiency, process of trench development, and usage methods are descrived.

1 Introduction

One of the important problems in the beach stabilization and the effective utilization of beaches is how to control wind-blown sand. Different types of countermeasures are employed in different parts of the world depending on the local conditions at the beach, such as weather, sea, and geographical conditions as well as the economical importance of the region. At the latest ICCE (25th), Hotta and Horikawa (1996) proposed a new type of prevention work, a sand trapping trench, for controlling wind-blown sand. The trench is given a rectangular shape with a depth of more than 1 m and a width of around 5 or 6 m by excavating the backshore of the beach (see Fig. 1). However, the details of trench could not be described in the paper since the main focus of the paper was not to discuss the trench itself. The purpose of this paper is to report the design and use of the trench in more detail.

2 Procedure

2.1 Background and Process of Trench Development

The idea of a sand trapping trench for controlling wind-blown sand stems from the results of several previous studies.

Inspiration to the trench came from an early paper that described a case where cultivated land close to a sandy beach was protected from wind-blown sand by excavating a stream upwind the beach, letting sand grains fall into the stream, and then returning the sand to the sea (Iwagaki, 1950).

Considering this case, Horikawa et al. (1983, 1984) tried to measure the sand transport rate in the field by using trenches those were 1 m deep and several meters wide. Figure 2 shows examples of the sand accumulation process in the

[1]Dept. of Const. Eng., Nihon Univ., 7-24-1, Narashino-dai, Funabashi, Chiba 274-8501, Japan
[2]Central Research Institute of Electric Power Industry, Abiko, Chiba, Japan
[3]Musashi Institute of Technology, Tokyo, Japan

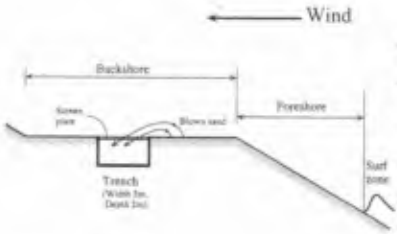

Fig. 1 Conceptional sketch of trench trap.

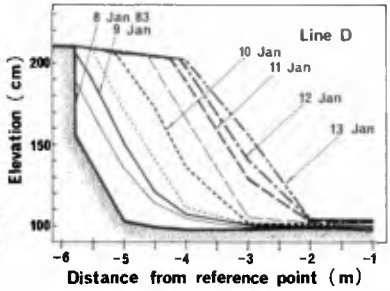

Fig. 2 Sand accumulation in the trench. (copied from Horikawa et al., 1984)

(a) Begining of the observation.

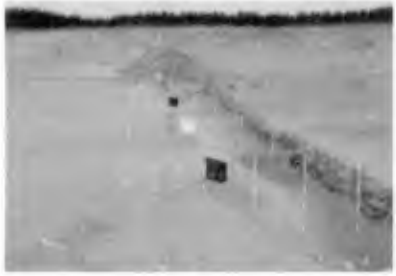

(b) After 5 days.

Photo 1 Trench trap used on a real beach.

trench and Photo 1 shows the trench (a) at the beginning of the observation., and (b) at the same location after 5 days. Figure 2 and Photo 1 show that the blown sand that fell into the trench was deposited at the upstream edge of trench with the deposition progressing in the downstream direction. The same level was maintained with respect to the beach surface and the rest angle of dry sand determined the downwind slope. This form of accumulation can be understood when we realize that a portion of the blown sand moves with the surface creep motion and that the flying distance of sand grains in saltation is rather short. Horikawa et al. (1983, 1984) also reported that no significant amount of sand was transported beyond the trench and they concluded that the trench could trap almost 100 % of the blown sand.

Using a large wind tunnel, Hotta and Horikawa (1993) measured the flying distance of blown sand in saltation motion. Figure 3 shows examples of observed distributions of falling sand grains. The falling rate was measured by a horizontal distribution-type trap that was 1 m long in the wind direction.

At the downwind end of the trap, a stainless wire net with a mesh of 75 μm was stretched vertically to a height of 30 cm. In Fig. 3, the solid curves are predictions obtained from the modified equation of the vertical distribution of sand transport rate by wind derived by Kawamura (1951). A large amount of sand grains falls a distance of 20 cm downwind from the end of the sand bed. The falling rates at locations 80 cm and 90 cm somewhat increase compared to the value at location 70 cm and deviate upwards from the predicted curve when the shear velocity becomes larger. This was caused by the fact that the flying sand grains hit the end-net and fell into the trap. Sand grains associated with this increase in amount are probably those that would fly beyond 1 m in the horizontal direction if not trapped. Therefore, we must recognize the fact that some amount of sand grains fly beyond 1 m in the horizontal direction. However, considering the fact that over 90 % of the total amount of wind-blown sand is transported below the elevation of 15 cm in a range of the shear velocity from 30 cm/s to 100 cm/s, we can safely assess that the flying distance for an amount of over 90 % of the total transported sand will be smaller than 1 m.

Using a horizontal distribution-type trap similar to the trap used by Hotta and Horikawa (1993), but enlarged to be 50 cm wide and 2 m long, Shiozawa et al. (1993) measured the flying distance of blown sand at a real beach. The result of the measurements is shown in Fig. 4. Figure 4 shows that the theoretical curve of flying distance of blown sand grains modified from Kawamura's equation can predict the observed data well and that the flying distance is smaller than 1 m in the horizontal direction for a shear velocity of about 29 cm/s. In the field measurements, a trench was used that was 1.5 m deep and 5.0 m wide. Shiozawa et al (1993) also reported that sand was transported beyond the trench for strong winds but the amount transported was negligible small compared to the amount trapped in the trench. The values of the transported and trapped sand and the wind speed were not given in the original paper.

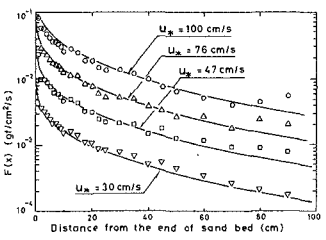

Fig. 3 Examples of horizontal distribution of falling sand grains. (copied from Hotta and Horikawa, 1993)

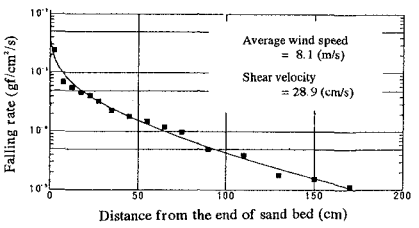

Fig. 4 Flying distance of blown sand grains observed in the field. (redrawn from Shiozawa et al., 1993)

Based on the investigations discussed above, the present authors concluded that the trench could be employed as a prevention work for wind-blown sand and proposed to use the trench practically in the field.

2.2 Remaining Problems and Study Subject

It is highly probable that over 90 % of blown sand will be trapped in the trench, if the trench has a length of about 2 m in the wind direction (hereafter we refer to the length as the width of trench), for shear velocities lower than 100 cm/s on sand surfaces with a grain size of around 0.3 mm. However, the field experiments carried out by Horikawa et al. (1983) also showed that the wind rushed onto the downwind edge of the trench and a violent disturbance of the flow field was generated in the case of a trench wider than 7 m. Thus, it was found that a trench too wide would not be good for stabilizing trapped sand. To solve this problem, the present authors carried out a wind tunnel experiments together with numerical simulations to determine a suitable width of the trench from the flow conditions in an open cavity (of similar shape). The main objective of this work was to find a suitable aspect ratio of the open cavity, where the aspect ratio is defined by the ratio of width to height of the open cavity. In the following sections, the wind tunnel and numerical experiments will be described.

3 Wind Tunnel Experiment

The wind tunnel experiments consisted of two parts, namely one part that was a tracer experiment to visualize the flow pattern inside the trench and an other part that encompassed measurements of wind speed to determine the wind speed field.

3.1 Facilities

The wind tunnel used in the experiments was a blow-off type with a test section having dimensions of 1.1 m high, 1.0 m wide, and 20 m long. To provide an open cavity (trench), the tunnel floor was fixed by wooden boards as shown in Fig. 5. An arbitrary aspect ratio could be selected by changing the width of the cavity.

Wind speed was measured with an array of hot-film anemometers consisting of twelve anemometers. The output from the amplifier unit of the anemometers was recorded and analyzed on a personal computer. The sampling interval of data was 1 Hz. The hot-film anemometer was omni-directional. Therefore, it was not possible to detect the wind direction.

For the tracer experiment, four 8 mm video cameras, including two digital-type and two high grade conventional-type cameras, were employed. The num-

ber of cameras used depended on the width of the cavity and the spatial range photographed by a camera varied from 20 cm to 60 cm.

Styrofoam particles with diameters ranging from 0.1 mm to 0.3 mm were employed as tracers. The specific gravity of the particles was about 0.02.

3.2 Experimental Procedures

The tracer experiment was carried out first. While blowing the wind and operating the cameras, the tracer was injected at different elevations through a pipe with an inner diameter of 25 mm that was lowered from the ceiling into the tunnel at a location 1 m upwind from the upwind edge of the cavity. The elevations of injection varied from the bottom to near the ceiling. A run continued until we could roughly sketch the flow pattern using visual observations. For one aspect ratio, tracer experiment was done for three reference wind speeds around 5 m/s, 10 m/s, and 15 m/s. The employed aspect ratios were 2, 4, 5, 6, 8, 10, and infinity (step down).

After finishing the tracer experiment, the vertical distribution of the wind speed was measured at locations where we judged that it was needed based on the tracer experiment. The measuring period of wind speed was 2 min at a location and data series encompassing 120 values was taken. The average of the wind speed at the point was then calculated. The complete wind field was also measured for three reference wind speeds.

3.3 Results and Discussions

Before discussing the results, we should keep in mind the limitations of this experiment.

The wind speeds employed, 5, 10, and 15 m/s, are prototype-scale. However, the floor surface consisted of a wooden board and the roughness of the surface

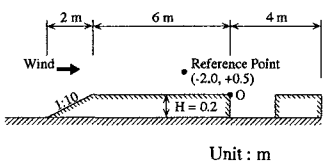

Fig. 5 Floor configuration for experiments.

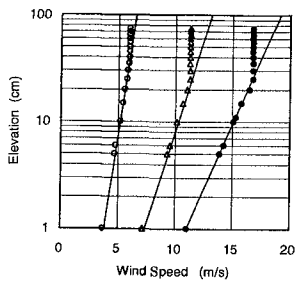

Fig. 6 Vertical distribution of wind speed.

was smaller than that at real beaches. The length scale becomes 1/5 or smaller than 1/5 if we assume that a trench will be employed in the field that has a depth of 1 m or more. The model experiment was carried out at a distorted scale, making it difficult to define a characteristic Reynolds number for the experiment. If we choose the depth of the trench, 0.2 m, as the characteristic dimension, Reynolds number becomes about 6.7×10^4, 1.3×10^5, and 2.0×10^5, for wind speeds of 5, 10, and 15 m/s, respectively, where the kinematic viscosity is taken as $1.5\times10^{-5}\mathrm{m}^2/\mathrm{s}$.

The tracer employed was light but still had some weight; therefore, the tracer tended to fall down to the floor. However, the flow patterns drawn from scattered tracers were almost the same for the three reference wind speeds, although the figures are not shown here because of space limitations.

The aim was to use a constant wind speed during the experiment. However, the wind speed fluctuated on the average about ±3.0 % due to the mechanical characteristics of the tunnel. Figure 6 shows the vertical distribution of the averaged wind speed above the wooden board floor. The logarithmic law is satisfied under an elevation of about 30 cm and the wind speed becomes constant at elevations higher than 30 cm. The reference wind speeds, 5, 10, 15 m/s are the wind speeds measured at the reference point (-2.0 m, +0.5 m) in Fig. 5 in the constant wind speed region. The wind speed measured was normalized by these reference speeds. The vertical distribution of the normalized wind speed at each location was the same for three of the reference wind speeds within the experimental error. Based on the above observations, the following discussion of the results is presented with reference to the flow patterns and the normalized wind speed field averaged for three of the reference wind speeds.

Figure 7 shows the flow patterns and the wind speed profiles. Allows showing the flow pattern are loci of tracers and do not mean wind velocity vectors. Attention is draw to Fig. 7 (b) showing the tests with aspect ratios of 6, 8, and 10 and the back step flow. The horizontal distance is reduced with a scale of 1/2 in these tests differentiating them from what is presented in Fig. 7 (a). In the back step flow the stagnation point appeared at a location of about 7.2H downwind the upwind edge of the cavity (from the origin). Many previous wind tunnel experiments or numerical simulations show that the stagnation point appears in a region about 7.0H to 7.5H. Therefore, it is considered that the present experiment provided reliable results in agreement with previous studies. The stagnation point shifts upwind to 6.8H for B/H = 10.0, to 5.8H for B/H = 8.0, and to 5.2H for B/H = 6 in the presence of a downstream wall so that an open cavity is formed. No stagnation point appears for B/H = 4.0, and for B/H = 5.0 it was difficult to establish the existence of a stagnation point in the visual observations during the experiment or on the video movie analysis. Considering these observation and looking closer at the flow patterns we can conclude that the main flow lowered downward due to the cavity touches

the bottom of the cavity and rushes onto the downwind wall of the cavity for aspect ratios larger than 6.0. The return flow from the downwind wall probably generates a violent disturbance in the cavity, and this result agrees with our field experience. A circulation cell exists for aspect ratios smaller than 5.0.

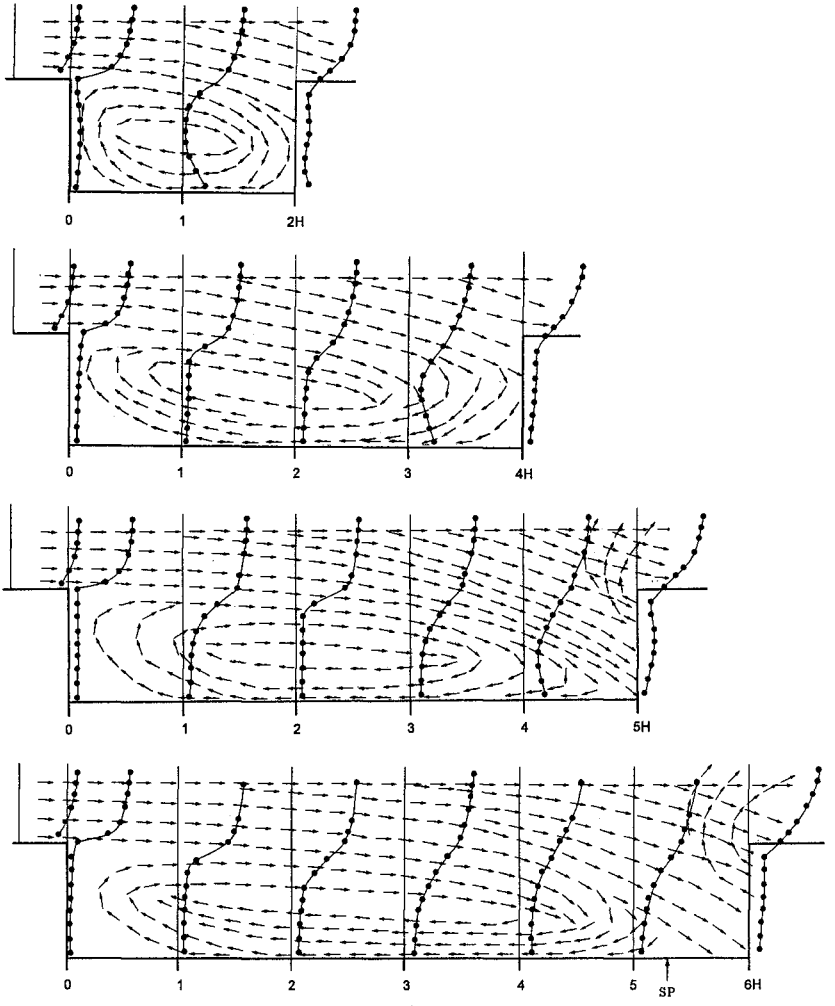

(a)

Fig. 7 Flow patterns and wind speed profiles. (SP : stagnation point)

At a first glance on the wind speed profiles it is difficult to directly find any particular features of the flow. However, careful investigations of the profiles together with the overall flow pattern allowed us to quantitatively establish the

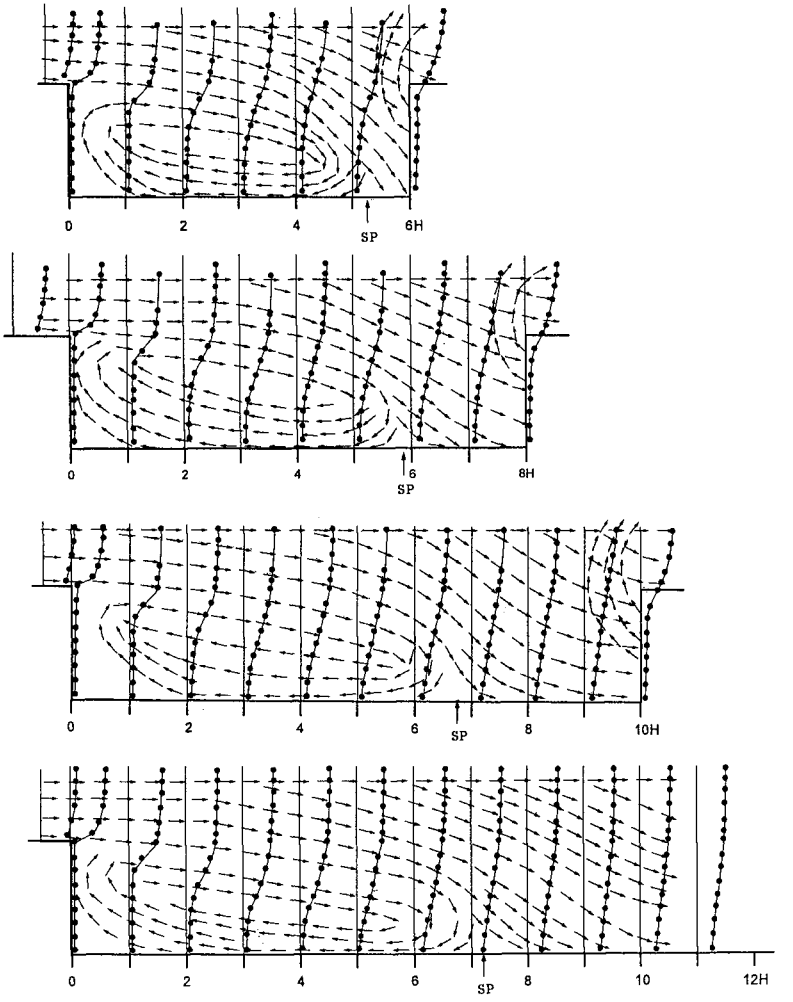

(b)

Fig. 7 Flow patterns and wind speed profiles. (SP : stagnation point)

flow characteristics. Figure 8 shows curves of equal wind speed in the cavities. From Fig. 8 we can perceive that the wind speed inside the cavity becomes stronger when the aspect ratio increases. To evaluate the wind speed conditions, we focus on the curves that have a value of 0.5 for equal wind speed. It is seen that the lowering of the curve valued at 0.5 into the cavity becomes larger when the aspect ratio becomes larger than 5.0. Based on the above discussion of the results, the present authors conclude that the aspect ratio should be smaller than 5.0 to keep low-disturbance conditions inside the cavity.

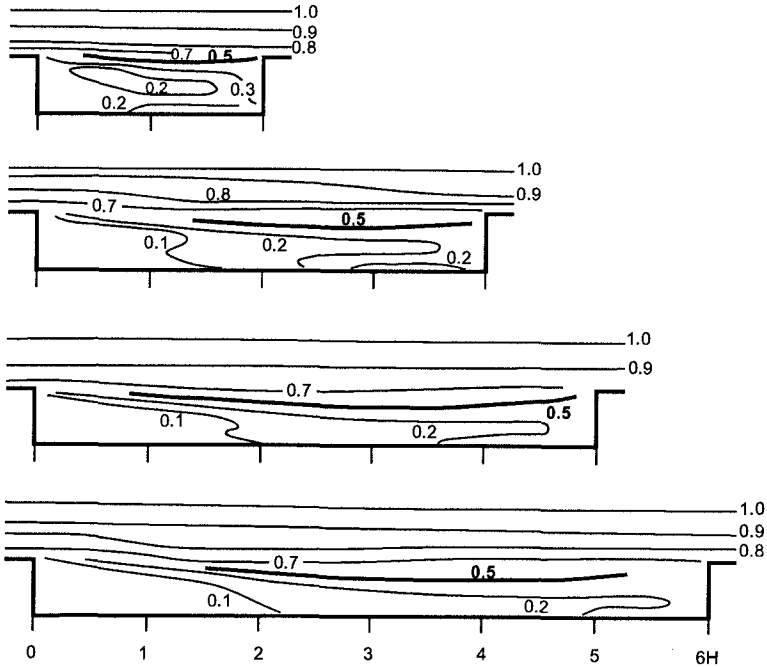

(a)

Fig. 8 Equal wind speed curves in the cavities.

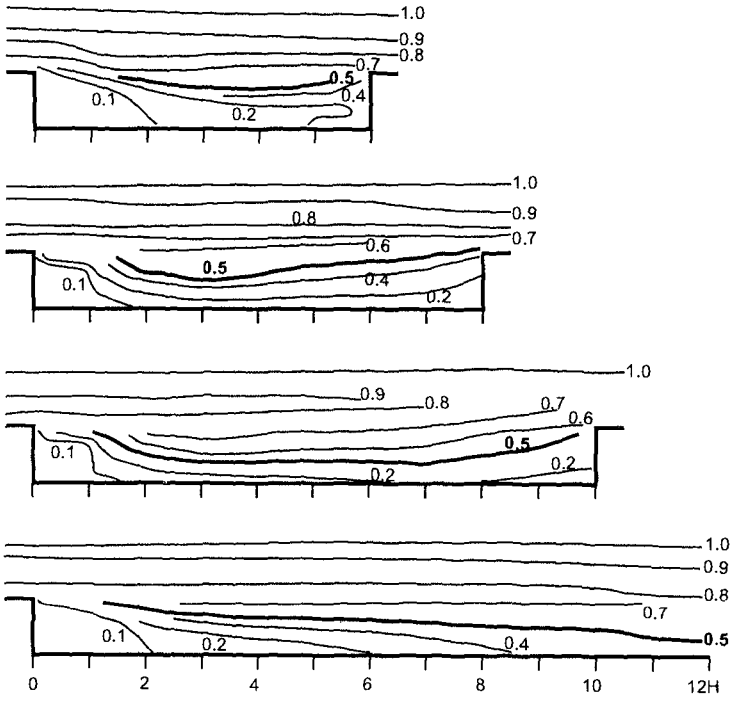

(b)

Fig. 8 Equal wind speed curves in the cavities.

4 Numerical Experiment

4.1 Basic Equations

In order to theoretically examine the results obtained in the experiments, we performed numerical simulation of the air flow in the trench trap. Since the fluid under consideration can be treated as an incompressible viscous fluid and the flow is a fully developed trubulent flow, the time-dependent Reynolds-averaged Naview-Strokes equation were selected together with the $k-\varepsilon$ modeling equations as the basic equations of the simulation. The equations can be written in

the following form.

$$\frac{\partial U_i}{\partial x_i} = 0 \tag{1}$$

$$\frac{\partial U_i}{\partial t} + U_j \frac{\partial U_i}{\partial x_j} = -\frac{1}{\rho}\frac{\partial P}{\partial x_i} + \frac{\partial}{\partial x_j}\left\{(\nu + \nu_t)\left(\frac{\partial U_i}{\partial x_j} + \frac{\partial U_j}{\partial x_i}\right)\right\} \tag{2}$$

$$\frac{\partial k}{\partial t} + U_j \frac{\partial k}{\partial x_j} = \frac{\partial}{\partial x_j}\left\{\left(\nu + \frac{\nu_t}{\sigma_k}\right)\frac{\partial k}{\partial x_j}\right\} + G - \varepsilon \tag{3}$$

$$\frac{\partial \varepsilon}{\partial t} + U_j \frac{\partial \varepsilon}{\partial x_j} = \frac{\partial}{\partial x_j}\left\{\left(\nu + \frac{\nu_t}{\sigma_\varepsilon}\right)\frac{\partial \varepsilon}{\partial x_j}\right\} + \frac{\varepsilon}{k}(C_{\varepsilon 1}G - C_{\varepsilon 2}\varepsilon) \tag{4}$$

$$\nu_t = C_\mu \frac{k^2}{\varepsilon} \tag{5}$$

$$G = \nu_t \left(\frac{\partial U_i}{\partial x_j} + \frac{\partial U_j}{\partial x_i}\right)\frac{\partial U_i}{\partial x_j} \tag{6}$$

Here, U_i and is the local time-averaged velocity components and P is the pressure, k and ε are the turbulent kinetic energy and its dissipation rate, respectively. ν is the kinematic viscosity, ν_t is the turbulent eddy viscosity, and G in the k and ε equations is the turbulence production term. The values of the constants $C_\mu, C_{\varepsilon 1}, C_{\varepsilon 2}, \sigma_k, \sigma_\varepsilon$ used in the turbulence model are $0.09, 1.44, 1.92, 1.0, 1.3$, respectively.

This formulation, however, is known to give poor predictions of turbulent characteristics when excessive generation of turbulent energy leads to a too high turbulent viscosity. To overcome this, Kato and Launder have presented a modified $k-\varepsilon$ model. Let the dimensionless strain parameter S and vorticity parameter Ω be defined according to :

$$S = \sqrt{\frac{1}{2}\left(\frac{\partial U_i}{\partial x_j} + \frac{\partial U_j}{\partial x_i}\right)^2} \tag{7}$$

$$\Omega = \sqrt{\frac{1}{2}\left(\frac{\partial U_i}{\partial x_j} - \frac{\partial U_j}{\partial x_i}\right)^2} \tag{8}$$

From eq.(6), it is easily verified that the energy production term may be rewritten :

$$G = \nu_t S^2 \tag{9}$$

Near a stagnation point, the very high value of S leads to the excessive levels of G. However, the vorticity parameter Ω near a stagnation point becomes nearly equal to zero since the deformation is nearly irrotational. Thus the replacement,

$$G = \nu_t S \Omega \tag{10}$$

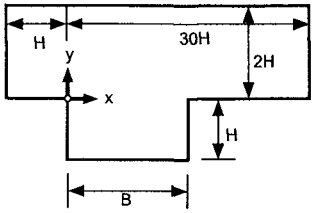

Fig. 9 Definition sketch of the computational domain.

gives a substantial reduction of G in the region around the stagnation point. This method has been found to give satisfactory predictions in the computation of turbulent flows. The modification is no remedy for the weakness in the Bousinessq stress-strain hypothesis, but it does greatly improve the behavior in some flows.

The discretization strategy used in this study is the three-step Taylor/Galerkin method. The discretized formulations of the basic equations are omitted here due to the limited space. One can find more details about this strategy in the referencies Hatanaka et al. (1998) and Jiang. et al. (1993).

4.2 Results and Discussions

In the numerical simulations, the Reynolds number was fixed to 10^5 and simulations for two aspect ratios, $B/H = 4$ and 6,were carried out. Figure 9 shows a definition sketch of the computational domain. The computational domain is discretized using bi-linear isotropic quadratic finite elements. The finite element mesh used in both cases had 8,365 nodes and 8,160 elements.

Figure 10 shows the stream lines of the flow field for the case $B/H = 4$ and for the case $B/H = 6$. In the case $B/H = 4$, one can see that the primary vortex in the trench is large and that the main stream dose not flow into the trench. However, in the case $B/H = 6$, the primary vortex move upstream in the trench and the main stream flows into the trench trap. Moreover, a stagnation point can be observed in the case $B/H = 6$ whereas no stagnation point can be observed in the case $B/H = 4$. These are the same results as were obtained in the experiments and therefore it can be said that the observations made in experiments were verified by the numerical model.

5 Concluding Remarks

The dimensions that the newly proposed sand trapping trench needs to function well as a controlling device for wind-blown sand are a width of 2 m (at

least in proto-type) and an aspect ratio of width to depth (B/H) smaller than 5.0. However, for engineering use, when solving problems on real beaches, we must also consider the storage capacity for trapping sand and the removal of the trapped sand. The optimal width and depth of the trench depend on the maximum allowable volume of trapped sand and the frequency of removal of the trapped sand during the windy season. The sand volume that will be trapped can be calculated by using the Kawamura or Bagnold formulas with a reasonable accuracy for engineering purposes, if we can estimate the wind conditions at the site. Then, a suitable width and depth of trench can be chosen. In addition, we must consider the removal method of the trapped sand. It is reasonable to assume that trapped and stored sand will be removed by earthmoving construction machines such as power shovels and bulldozers. The dimensions and effectiveness of the earthmoving machines will be one of the factors that determines the width and depth of the trench. To preserve a safe environment for various activities on the beach, a cover made of screen or mesh plate should be placed on top of the trench. The opening ratio, defined as the ratio of the open space to the total project area of the plate, is also one of factors that determines the width of the trench; (this problem has not been studied yet). There are many problems to be solved in the practical use of trenches on beaches. The authors believe, however, that well-educated engineers can deal with them.

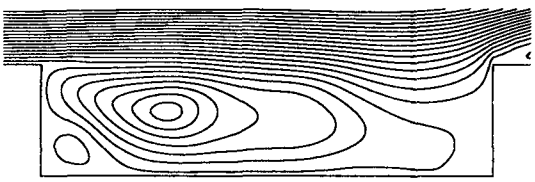

(a) B/H=4.0

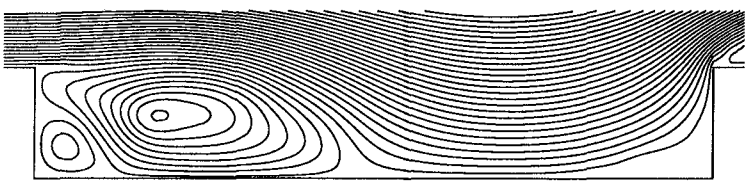

(b) B/H=6.0

Fig. 10 Stream lines of mean velocity field ($Re = 10^5$)

References

Hatanaka, K. and S. Hotta (1998) : Finite element analysis of air flow around permeable sand fences, Int. J. Num. Meth. Fluids, Vol. 24, pp. 1291-1306.

Horikawa, K., S. Hotta, S. Kubota and S. Katori (1983) : On the sand transport rate by wind on a beach, Coastal Eng. in Japan, Vol. 26, JSCE, pp. 101-120.

Horikawa, K., S. Hotta, S. Kubota and S. Katori (1984): Field measurement of blown sand transport rate by trench trap, Coastal Eng. in Japan, JSCE, Vol. 27, pp. 213-232.

Hotta, S. and K. Horikawa (1993) : Vertical distribution of sand transport rate by wind, Coastal Eng. in Japan, JSCE, Vol. 36, pp. 91-110.

Hotta, S. and K. Horikawa (1996) : Countermeasures against wind-blown sand on beaches, Proc. 25th, Coastal Eng. Conf., ASCE, pp. 4188-4199.

Iwagaki, Y. (1950): Sand drift by wind on the coast, Bulletin of the Disaster Prevention Research Institute, Kyoto University, No. 3, pp. 31-35. (in Japanese)

Jiang, C.B., K.Hatanaka, M.Kawahara and K.Kashiyama (1993), A Three-Step Finite Element Method for Convection Dominated Incompressible Flow, Computational Fluid Dynamics Journal, Vol.1, No.4, pp.447–466.

Kato, M. and B.E. Launder (1993) : The modeling of turbulent flow around stationary and vibrating square cylinder, Proc. of 9th Symp. On Turbulent Shear Flows, pp. 10-4-1 - 10-4-6.

Kawamura, R. (1951) : Study on blown sand by wind, Rep. of the Inst. of Science and Technology, Univ. of Tokyo, Vol. 5 (3/4) : pp.95-112 (in Japanese), English translation available in : Research Tech. Rep. HEL-2- 8, Hydraulic Eng. Lab., Univ. of Calif., Berkeley, 1964, pp. 38 (I.Nagahama and H. Hiraoka, translators).

Launder, B.E. and D.B. Spalding (1974) : The numerical computation of turbulent flow , Comput. Meth. Appl. Mech. Eng., Vol. 3, pp. 269-289.

Shiozawa, T., S. Nakayauchi, M. Akazawa, S. Tamashiro and K. Kuroki (1993) : Observation of the sand transport rate by wind at Niigata West Beach, Proc. of Coastal Eng., Vol. 40, JSCE, pp. 281-285. (in Japanese)